INORGANIC CHEMISTRY
FRONTIERS

CHINESE CHEMICAL SOCIETY
ROYAL SOCIETY OF CHEMISTRY

RESEARCH ARTICLE

View Article Online
View Journal

Check for updates

Cite this: DOI: 10.1039/d5qi01216c

Scrutinising ligand pre-reduction: unlocking pathways to mono-, homo-, and heterobimetallic naphthyridine diimine complexes

Adrian Jenner, Laura Neumüller, Hartmut Schubert, Cäcilia Maichle-Mössmer and Manfred Manßen *

Received 29th May 2025,
Accepted 6th August 2025

DOI: 10.1039/d5qi01216c

rsc.li/frontiers-inorganic

The redox-active naphthyridine diimine (NDI) framework serves as a versatile scaffold for synthesising monometallic as well as homo- and heterobimetallic complexes, owing to its electronic flexibility and rigid geometry. This comprehensive study investigates the influence of ligand pre-reduction on the reactivity and structural outcomes of NDI with alkali and alkaline earth metals. Systematic analyses reveal that the nature and extent of NDI reduction critically determine the resulting metalation pathways. Pre-reduction with sodium favors the formation of homobimetallic complexes, while lithium enables access to heterobimetallic architectures, and magnesium yields monometallic species. The use of pre-reduced NDI intermediates allows for salt metathesis reactions with group 13 halides, giving rise to well-defined Al–Al, Al–Li, Ga, and Ga–Li complexes. Structural and spectroscopic data provide insight into oxidation states and electronic delocalisation within the NDI framework. A metrical model, inspired by the chemistry of diazabutadiene ligands, is introduced to classify NDI redox states based on characteristic bond lengths. These results highlight the synthetic utility of pre-reduction strategies for tailoring the electronic and structural diversity of NDI-based complexes across a broad range of metals.

Introduction

Cooperativity in bimetallic complexes was revealed to be more common in homogenous catalysis than previously thought.[1–3] Especially during the last few years, interest in the interaction within bimetallic complexes grew in popularity as they are found in enzymes activating small molecules like dihydrogen and dinitrogen.[4,5] They also have proven to be highly versatile in bond activation as well.[6–8] Systematic approaches to generate such complexes with possible metal–metal interaction include the use of rigid or electronic flexible environments, by forcing interaction through close proximity, or redox-activity.[9] However, examples which make use of this remain scarce.[9,10]

One of these ligand classes of particular interest are redox-active naphthyridine diimines (NDIs, **I**).[11] The planarity of the naphthyridine-backbone and conjugated imine groups offer a rigid and electronic flexible setting (Scheme 1). Its great variety of oxidation states was first used and described in coordination chemistry by the group of Uyeda, who reported the successful synthesis of [{$Ni_2(C_6H_6)$}(NDI)] (**II-Ni**).[12–15] Implementing iron (**II-Fe**) and cobalt (**II-Co**), they report on all three complexes reacting in oxidative addition reactions with allyl chlorides,[16] and complex **II-Co** catalysing coupling reactions of tertiary alkyl azides to azoalkanes as well.[17] However, the synthetic protocols for these complexes highlight the challenges for the preparative methods and limitations to certain metals. Due to the relative softness of NDI, according to HSAB concepts, suitable metal(0) precursors are the best candidates for generating bimetallic NDI complexes. This becomes particularly evident for complex **II-Ni**, for which the Uyeda group utilises the reaction of NDI with $(COD)_2Ni(0)$ (COD = cyclooctadiene).[12] To address this limitation, an alternative strategy

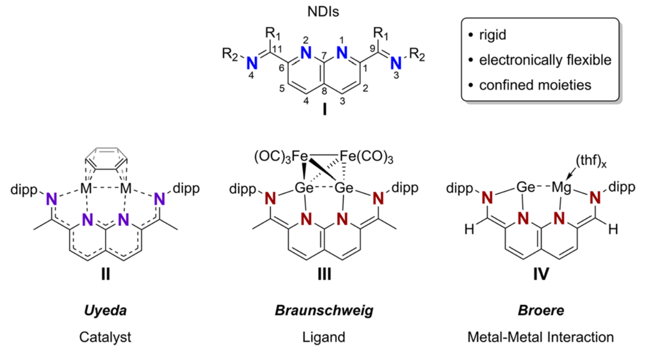

Scheme 1 Numeration of NDI and overview of previous work.

---

*Institut für Anorganische Chemie, Eberhard-Karls-Universität Tübingen, Auf der Morgenstelle 18, 72076 Tübingen, Germany.
E-mail: manfred.manssen@uni-tuebingen.de*

involves pre-reducing NDI in a separate initial step. This opens up the possibility for salt metathesis reactions, which makes it especially interesting for other metal precursors, which are considered as hard Lewis acids.

To obtain the complexes **II-Fe** and **II-Co**, the group of Uyeda used *in situ* generated dark brown/orange Na_2NDI by reducing NDI with sodium amalgam, and salt metathesis reaction.[16] Similarly, the group of Braunschweig was able to synthesise $[\{Fe(CO)_3\}_2\{Ge_2(NDI)\}]$ (**III**), which uses a binuclear NDI complex as a ligand. For this, they generated dark green Na_2NDI *in situ* by reducing NDI with sodium in NaCl, which differs from the dark brown/orange species described by Uyeda.[18] Additionally, the group of Broere achieved the synthesis of heterometallic binuclear complexes such as $[\{Mg(thf)_xGe\}(NBA)]$ (**IV**) (NBA = naphthyridine bisaldimine), in which the metal–metal interaction is a key focus.[19] To synthesise **IV**, NBA was reduced with magnesium, and subsequent salt metathesis reaction with $GeCl_2$-dioxane resulted in mononuclear [(Ge)(NBA)].[19] After further reduction with magnesium, they were able to isolate complex **IV**.

To overcome the synthetic limitations of this ligand class and to gain a deeper understanding of the reduction chemistry of NDI, we investigated the reactivity of strongly reducing alkali and alkaline earth metals in detail. In this context, we sought to broaden the range of possible metals that can be introduced to NDI or analogous systems for researchers working on elements across the entire periodic table. Here, we report comprehensively on the influence of the initial pre-reducing step to the ligand with spectroscopical, crystallographic, and structural data. Furthermore, we highlight changes in reactivity for the different alkali and alkaline earth metals, resulting in monometallic and homo-/bimetallic complexes of main group elements.

Results and discussion

Reduction with alkali metals

Reacting NDI with 3.3 equivalents of sodium amalgam in THF results in an initial change in colour to purple and ends with a dark orange/brown solution of *in situ* generated Na_2NDI. This has been used by the group of Uyeda in salt metathesis reactions with $FeCl_2$ and $CoCl_2$.[16] An approach from the group of Braunschweig includes the reduction using 3.4 equivalents of Na/NaCl in a mixture of THF and benzene. Here, the reaction results in a dark green solution of presumed Na_2NDI which was also used successfully in a salt metathesis reaction with $GeCl_2$·dioxane.[18]

To investigate the differences between the differently coloured solutions, the reduction of NDI was repeated using varying equivalents of metallic sodium. The deep green solution used by the group of Braunschweig was reproducible with a great excess of sodium in THF. But attempts to observe a distinct diamagnetic species in the ^1H NMR spectrum of this solution were unsuccessful, suggesting the presence of a mixture, including paramagnetic species. Performing the reduction in C_6D_6 with 2 equivalents of metallic sodium reproduces the orange/brown solution from the group of Uyeda. ^1H NMR spectroscopy was used for comparison, with the proton signals of the naphthyridine backbone proving particularly useful due to their well-resolved positions in the spectrum. Our results align with previous observations, showing two sets of upfield-shifted doublets (5.72 ppm and 4.61 ppm), which indicate a loss of aromaticity in the backbone.[16] A high dependency on the solvent is revealed by comparing the proton signals of the disodium reagent in C_6D_6 and in THF-d_8 (THF-d_8: 5.38 and 4.02 ppm, Fig. S1).

The *in situ* generated Na_2NDI cannot be isolated, as it is unstable as a solid even at −80 °C. Multiple attempts of crystallising this complex were unsuccessful, however quenching the solution with TMEDA (Scheme 2), acetonitrile or crown ether result in monoanionic NDI sodium compounds. The structure of $[Na(thf)_3(NDI)]$ (**1**) was confirmed by single crystal X-ray diffraction of red crystals obtained from a solution in THF (Fig. 1). Similarly, quenching the Na_2NDI in solution by

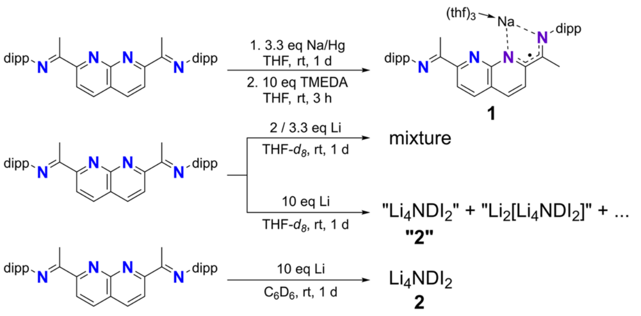

Scheme 2 Reaction of NDI with sodium amalgam and TMEDA, and with granular lithium.

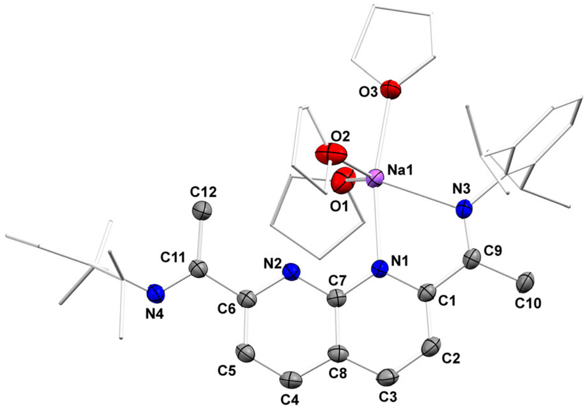

Fig. 1 Molecular structure of complex **1**. All atoms are represented by atomic displacement ellipsoids set at 50% probability. Solvent molecules and hydrogen atoms are omitted for clarity. Carbon atoms of the coordinating solvent and substituents are displayed in a capped stick model. Selected interatomic distances (Å): Na1–N1 2.360(2), Na1–N3 2.472(2), N1–C1 1.368(2), C1–C9 1.456(2), N3–C9 1.305(2), N2–C6 1.350(2), C6–C11 1.486(3), N4–C11 1.278(2), C2–C3 1.380(3), C4–C5 1.375(3), C7–C8 1.433(2).

addition of acetonitrile also results in a mononuclear compound **1-MeCN** (Fig. S32).

Immediately noticeable in the molecular structure of complex **1** is the flipped configuration of the nitrogen atoms in the unoccupied moiety of N2 and N4, which is also found in free NDI. Since both nitrogen atoms in each moiety are rigidly held in place by the NDI framework, the metal centre displays a distorted trigonal bipyramidal geometry. The Na–N1 bond (2.360(2) Å) is at the lower end of Na–N distances found in monometallic complexes of non-innocent monoanionic BIAN and NNN-pincer systems (2.33–2.52 Å).[20,21] The Na–N3 bond on the other hand is with 2.472(2) Å at the higher end of that range. Together with only slight changes for C1–C9 (1.456(2) Å) and N3–C9 (1.305(2) Å), the Na–N3 bond is primarily of dative nature.

With the purpose of investigating the influence of the metal used for reduction, reactions were also performed with granular lithium. Aiming for a "Li_2NDI", the reactions of the free NDI ligand with granular lithium in either THF-d_8 or C_6D_6 are shown in Scheme 2. Starting in THF-d_8 with 2 and 3.3 equivalents lithium – similar to the reaction with sodium – the reaction mixture turns from light yellow over dark brown to a dark orange solution. The ^1H NMR and EPR spectra of these reactions (Fig. S2 and Fig. S20) reveal a mixture of several dia- and paramagnetic species. The ^7Li NMR spectrum for 2 equivalents (Fig. 2b, top) consists of a broad signal at 0.00 ppm, overlapping with another broad signal at 1.33 ppm, hinting towards a more dynamic system. Using 10 equivalents of lithium, the reaction mixture continues to turn from a dark orange to a deep violet colour. The line broadening is even more apparent in the ^7Li NMR spectrum (Fig. 2b, middle) with several overlapping signals at 1.79, 1.18 and 0.10 ppm. This indicates strong dynamics for the lithium nuclei, which could be explained by the exchange of the $Li(thf)_4$ fragment. In sharp contrast, the ^1H NMR spectrum (Fig. S3) is comparable to the spectrum after reduction of NDI with sodium, suggesting full conversion: the proton signals of the naphthyridine-backbone show an up-field shift. However, this shift is most prominent for sodium (Fig. 2a, bottom). It is less pronounced in the case of lithium, where they are only shifted to 4.83 ppm. This indicates a loss of aromaticity in both complexes, and consequently higher diene characteristics.

The dynamic nature of the reaction of NDI and lithium is also reflected in the crystallographic data with diverse structural motifs (Fig. 3). Reacting NDI with 2 equivalents of granular lithium (Scheme 2), and layering the solution with *n*-pentane, orange-red crystals of $[Li(thf)_4][\{Li\}_3(NDI)_2]$ (**2a**) can be isolated. Dark green crystals of $[\{(Li)_3(Li(thf))\}(NDI)_2]$ (**2b**) are obtainable from the reaction with 10 equivalents. Both complexes are dimeric NDI structures with varying lithium cores and resemble different delocalised C–N systems, such as diazaallyl (**2a**) and diazabutadiene (**2b**) complexes. In complex **2a**, a Li_3-core is located in between two NDI units, with a fourth one being solvated by four molecules of THF in the periphery. Therefore, each NDI unit possesses a charge of −2. For Li1, a σ-coordination to the pyridine N1 and the imine N3, as well as a η^3-coordination to N1′–C7′–N2′ to the other NDI unit can be found. Coordination for Li3 is analogous to Li1. For Li2, the lithium atom is two times σ-coordinated (N2 and N4, N2′ and N4′). The core of complex **2a** appears to have formed from a Li_2NDI and a LiNDI fragment, where the unoccupied moiety of LiNDI coordinated a lithium centre of Li_2NDI. Complex **2b** on the other hand contains a Li_4-core, which forms a regular diamond shape with an edge length of around 2.66 Å. In this shape, Li1 is coordinated by one molecule of THF, and all four pyridine nitrogen atoms (N1, N2, N1′, N2′). An η^4-coordination is found for Li2 to N1–C1–C9–N3, and Li3 being equivalent to that. This coordination is indicative of significant delocalisation along these bonds. Aside from **2b**, additional crystals of a compound with the molecular formula $[Li(thf)_4]_2[Li_4NDI_2]$ (connectivity, Fig. S36) further proof the poor selectivity of these reactions (Scheme 2).

Since coordinating solvents seem to play an important role in the formation of compound **2**, the reactions were also per-

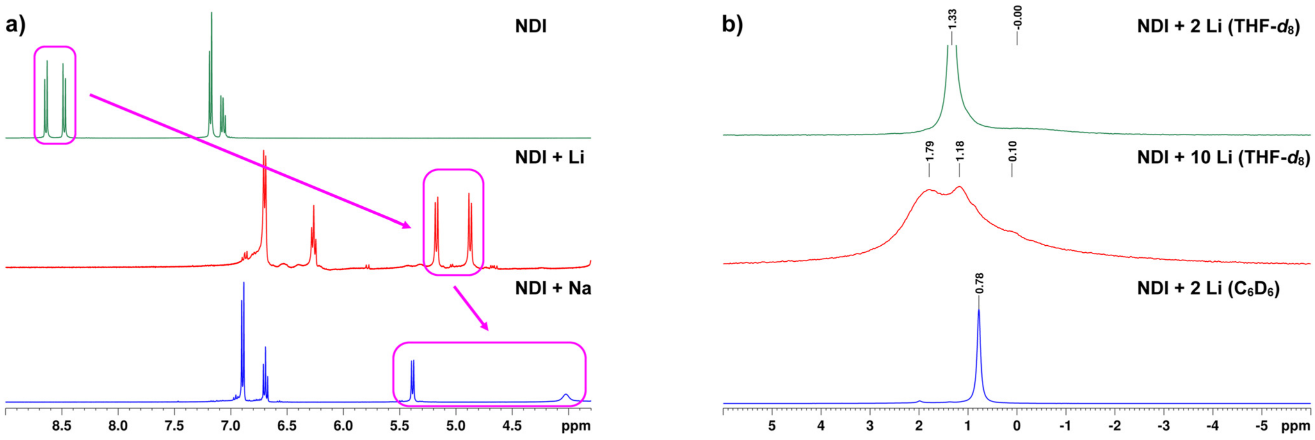

Fig. 2 (a) ^1H-NMR spectra in THF-d_8 of NDI (top), NDI with 10 equivalents of granular lithium (middle) and NDI with 2 equivalents of sodium metal (bottom). Marked (magenta) are the proton signals of the protons at C3 and C4. (b) ^7Li-NMR spectra of the reaction mixtures of NDI and granular lithium with 2 equivalents in THF-d_8 (top), with 10 equivalents in THF-d_8 (middle), and with 10 equivalents in C_6D_6 (bottom).

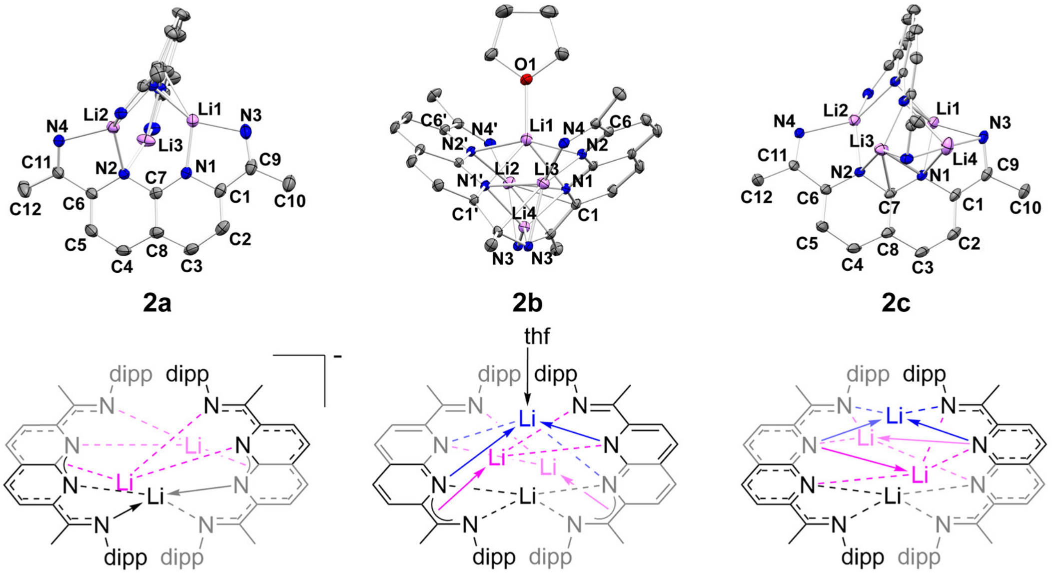

2a **2b** **2c**

Fig. 3 Molecular structure of complexes **2a–2c** (top). All atoms are represented by atomic displacement ellipsoids set at 50% probability. Solvent molecules, hydrogen atoms, and carbon atoms of the substituents, as well as a $[Li(thf)_4]^+$ fragment for complex **2a** are omitted for clarity (for metrics, see SI). Schemes corresponding to complexes **2a–2c** to visualise binding situation (bottom).

formed in a non-coordinating solvent. The reaction of NDI with 10 equivalents of granular lithium in C_6D_6 (Scheme 2) starts out similar to the one in THF-d_8. But instead of turning deep violet at the end of the reaction, it turns deep brown in colour. The ^{1}H NMR spectrum for the reaction mixture (Fig. S4) is comparable to the one in THF-d_8. The shift of proton signals of the naphthyridine-backbone is present as well (4.87 ppm), but not as pronounced. A difference is observable in the ^{7}Li NMR spectrum (Fig. 2b, bottom). The spectrum consists of a sharp signal at 0.78 ppm with no extensive broadening. Another remarkable detail is that neither prolonged reaction time nor re-dissolving after removal of the solvent *in vacuo* change the spectra obtained. Cooling down a solution from the reaction of NDI and 10 equivalents of lithium in C_6D_6 results in brown crystals of $[(Li)_4(NDI)_2]$ (**2c**) (Fig. 3). The structural motif is similar to the one of complex **2b** with a Li_4-core. However, the core in complex **2c** forms a kite with edge lengths of around 2.45 Å and 3.00 Å. Such oligomeric structures are known to form for lithium amide and imide complexes.[22,23]

Comparing these structural motifs of complexes **2a–2c** altogether, complex **2a** seemingly resembles the reduction to a "Li_2NDI" compound, where the formation of a Li_4-core was incomplete. Depending on the solvent, the complete formation leads to a mixture with complex **2b** as major product in THF-d_8 and selectively to complex **2c** in C_6D_6. Consequently, for our further reactivity studies, we chose the selective formation of complex **2c** in aromatic solvents (*vide infra*).

After investigations of the reaction with lithium and the more elusive reaction with sodium, efforts in reducing with potassium were also made. Reacting NDI with an excess of potassium results in a single change of colour to dark red-brown. Analytics of this product are inconclusive, regarding the degree of reduction. The EPR spectrum (Fig. S18) of the frozen solution in THF at 123 K shows a singlet at $g = 2.0017$, indicating an organic ligand based radical species. When the reaction is carried out with 2 equivalents of metallic potassium and analysed by ^{1}H NMR spectroscopy, no signals corresponding to a diamagnetic species are observed. Since the analogous reactions with lithium and sodium yield diamagnetic products, the formation of a 'K_2NDI' complex can be ruled out—despite elemental analysis of the product (see SI) being most consistent with $[K_2(thf)_2(NDI)]$. Other possible, less fitting matches include $[K_3(thf)(NDI)]$ and $[K(thf)_2(NDI)]$. Comparing the ionic radii of potassium (1.37 Å) and sodium (0.99 Å),[24] the spatial demand for a second potassium ion inside the moieties is far greater. However, it is also possible for a second potassium atom to coordinate on top of the moieties, to the two nitrogen atoms of the naphthyridine. Such a motif is known for the complex $[\{Ni_2(C_6H_6)\}\{K(thf)_3\}(NDI)]$, described by the group of Uyeda.[16] Assuming one potassium ion is located within the moiety, and a second is present as a $K(thf)_3$ fragment coordinated above it, the third potassium ion is likely a solvated species, given the limited available space. It appears unlikely that nearly all coordinated THF molecules would be lost through volatility to yield a composition such as $[K_3(thf)(NDI)]$. Therefore, $[K(thf)_2(NDI)]$ represents the most reasonable formulation. Unfortunately, efforts of crystallising from different solvents and mixtures of solvents, as well as addition of cryptands did not yield any results.

Reduction with alkaline earth metals

In contrast to the visible reaction of NDI with alkali metals, using magnesium shavings as a reducing agent requires several weeks at ambient temperature (Scheme 3). After four weeks in THF and washing with *n*-pentane (see SI), [Mg(NDI)$_2$] (**3**) can be isolated as a red powder and crystallised from cooling down a solution in THF (Fig. 4). Here, one metal centre occupies one moiety of each of the two NDI units and not both moieties of only one unit. The magnesium atom, located on the crystallographic inversion centre, is coordinated by two NDI units. The mean planes of the naphthyridine-backbones are tilted by 74.7°. The distorted tetrahedral geometry at the magnesium centre becomes apparent looking at the N3–N1–N1′–N3′ dihedral angle of 91.5°. Since only one moiety per NDI is occupied, the nitrogen atoms of the second moiety have a flipped conformation, similar to compound **1**. The Mg–N1 and Mg–N3 bonds (2.028(1) Å and 2.104(1) Å) are within the expected range of 1.966–2.111 Å of diazabutadiene (DAD) magnesium complexes.[25–27]

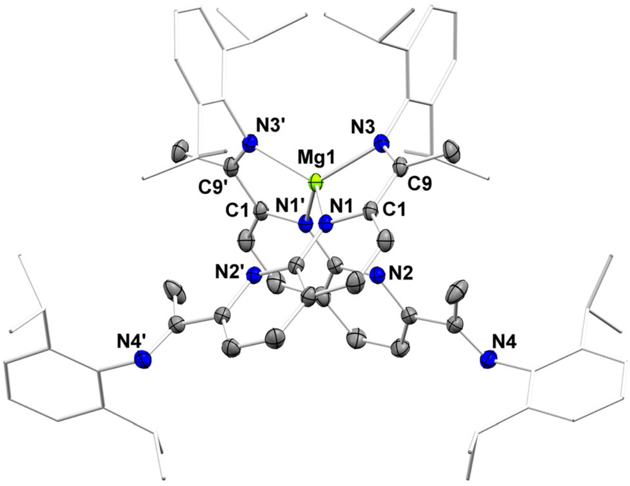

Fig. 4 Molecular structure of complex **3**. All atoms are represented by atomic displacement ellipsoids set at 50% probability. Solvent molecules and hydrogen atoms are omitted for clarity. Carbon atoms of the substituents are displayed in a capped stick model. Selected interatomic distances (Å): Mg1–N1 2.028(1), Mg1–N3 2.104(1), N1–C1 1.371(2), C1–C9 1.440(2), N3–C9 1.326(1), N2–C6 1.337(2), C6–C11 1.490(2), N4–C11 1.278(2), C2–C3 1.385(2), C4–C5 1.385(2), C7–C8 1.425(2) (for further metrics, see SI).

The cw-EPR spectrum of a frozen solution of compound **3** in THF at 123 K (Fig. 5a) features an intense central peak (330 mT, g = 2.004) and side bands, as well as a transition at half-field (165 mT, g = 4.008). The transition at half-field is characteristically found for group spins $S > \frac{1}{2}$, which matches the expected S = 1 system. A well-resolved cw-EPR spectrum of an Et$_2$O solution at 298 K (Fig. 5b) further reveals strong hyperfine couplings. Due to the resulting complex signal pattern, the values of the hyperfine coupling constants A for the simulation of the spectrum had to be based on calculations (see SI). Based on those values, hyperfine coupling to all eight nitrogen and at least six hydrogen nuclei is observable. Four of the nitrogen nuclei have equal hyperfine coupling constants, corresponding to the four nitrogen atoms bound to magnesium. The other nitrogen nuclei are two pairs of two equivalent nuclei. These can be assigned to the two free nitrogen nuclei in the naphthyridine-backbone, and two in the imine group, confirming the structure of complex **3** in solution. The absence of side bands in the EPR spectra when pre-reducing with lithium or sodium (Fig. S20 and Fig. S21) further supports the structural difference.

In order to reduce the reaction time of NDI and magnesium, which is due to the low solubility of magnesium in THF, the more accessible Mg(anthr)(thf)$_3$ (anthr = anthracene) was used (Scheme 3, 12 h). Attempts to reduce the amount of by-product were made by employing an excess of *in situ* generated Mg(anthr)(thf)$_3$, wherein an excess of magnesium is activated with dibromoethane and combined with 0.1 equivalents of anthracene.[28,29] Interestingly, this reaction resulted in the formation of dark green [{Mg(thf)$_2$}$_2$(μ-Br)(NDI)] (**4**). In the ^{1}H NMR spectrum of complex **4** no diamagnetic species is apparent, only a singlet is observable in the cw-EPR spectrum in a frozen solution in THF at 123 K with g_{iso} = 2.0020 (Fig. S19).

Analysing the crystal structure (Fig. 6, top), the Mg–N bonds are similar to the ones found in compound **3**. The adopted geometry of the magnesium centre is a distorted trigonal bipyramid, like complex **1**, except of one in-plane THF molecule being replaced by the bridging bromide. A Mg–Mg bond can be excluded by comparing the Mg1–Mg2 distance of 3.761(1) Å.[30,31] The possibility of two Mg(I) centres can therefore be dismissed. With a mirror plane through the C7–C8

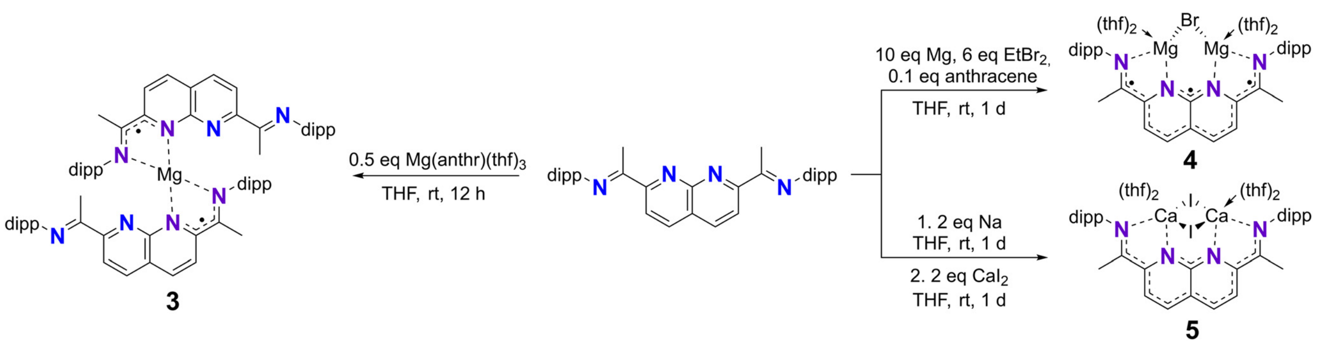

Scheme 3 Reactions of NDI with neat, and *in situ* generated Mg(anthr)(thf)$_3$, as well as salt metathesis reaction with CaI$_2$ after pre-reducing with sodium.

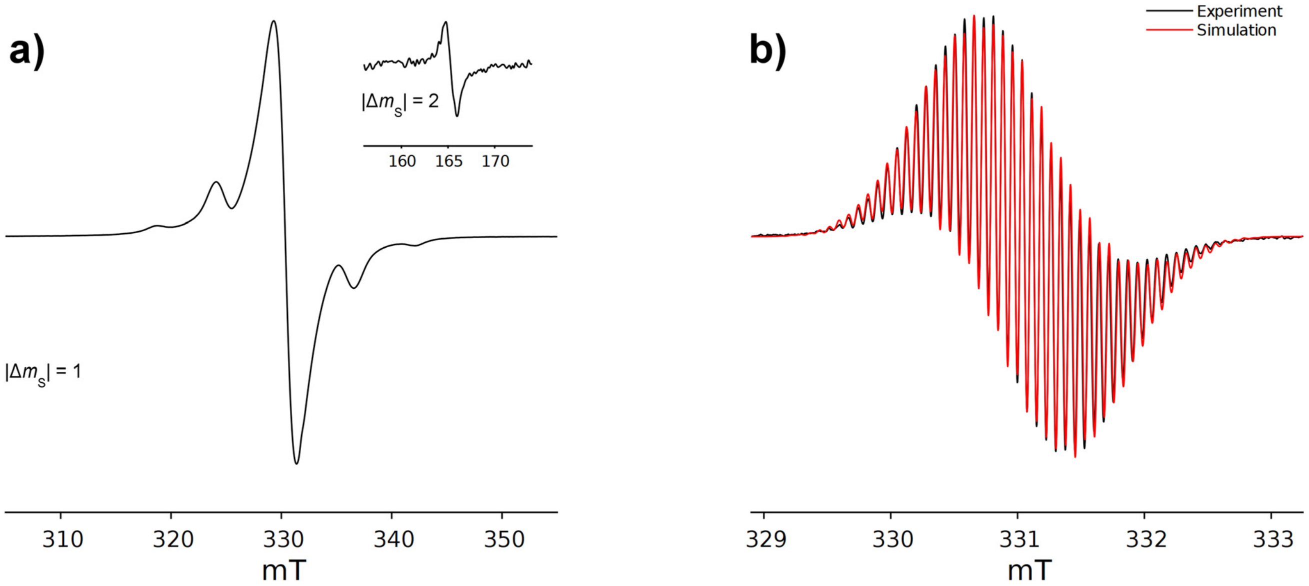

Fig. 5 (a) EPR (X-Band, ν = 9.2564 GHz) spectrum of a frozen solution of compound **3** in THF at 123 K ($|\Delta m_s| = 1$ region) with an inlay of the $|\Delta m_s| = 2$ region. (b) Experimental EPR spectrum (X-Band, ν = 9.2564 GHz) and simulated spectrum of a solution of compound **3** in Et_2O at 298 K. Parameters for the simulation: $S = 1$, $g = 2.00715$, Gaussian line width (lwpp) = 0.05 mT, (4*) A_N = 4.23 MHz, (2*) $A_{N'}$ = 2.12 MHz, (2*) $A_{N''}$ = 1.07 MHz, (6*) A_H = 10.70 MHz.

bond, mixed oxidation states of Mg(I) and Mg(II) seem unlikely to result such a symmetrical molecular structure. This suggests that both magnesium centres reside in the formal oxidation state of +2 with a trianionic $[NDI]^{3-}$ fragment. A closer look at the N3–C9 and C1–C9 bonds reveals bond lengths differing from the $[NDI]^{1-/2-}$ fragments found in other NDI complexes, but close to the ones reported for the $[NDI]^{4-}$ fragment in Ge_2NDI,[18] 1.384(4) Å and 1.388(4) Å *versus* 1.365 Å and 1.384 Å. This will be discussed in more detail at a later point (*vide infra*). What sets the tetraanionic NDI fragment apart from the other anionic states is the C7–C8 bond (1.451(5) Å for compound **4**, 1.397(3) Å for Ge_2NDI). As a consequence of the four additional charges, there are only slight contributions of a single bond, resulting in a relatively short C7–C8 bond length. Altogether, spectroscopical and structural data suggest two Mg(II) centres and a trianionic NDI fragment.

Since the reactions with magnesium differed from those with the alkali metals, similar reactivity studies were also undertaken with calcium. However, direct reduction of NDI using metallic calcium did not result in any reaction. Consequently, a route *via* salt metathesis was employed by generating the disodium reagent *in situ* in THF (Scheme 2), followed by the addition of 2 equivalents of CaI_2, which yielded $[\{Ca(thf)_2\}_2(\mu\text{-}I)_2(NDI)]$ (**5**). The ^1H NMR spectrum of complex **5** in THF-d_8 (Fig. S5) seems at first glance in favour of a C_{2v}-symmetric species in solution. Two sharp doublets of the characteristic upfield shifted protons of the naphthyridine-backbone are observable at 6.09 ppm and 4.86 ppm in agreement with a symmetric homometallic complex. A closer look at the signals corresponding to the dipp substituents reveals limited rotation. The signals corresponding to the CH_3 protons of the *i*Pr groups are found as a multiplet at around 1.20 ppm. The broad singlet at 3.11 ppm of the C*H* protons of the *i*Pr groups further illustrates the restricted rotation. The inequality of the two metal centres differentiates complex **5** from the other homometallic binuclear NDI complexes, which is further supported by the crystal structure of complex **5** (Fig. 6, bottom).

Even though both metal centres display a distorted octahedral geometry, the N2–Ca1–N4 plane is tilted by 22.93° out of the N2–C6–C11–N4 mean plane, whereas N1–Ca2–N3 is coplanar with the N1–C1–C9–N3 mean plane (0.68°). This is due to the steric demand of the Ca(II) cations (1.00 Å) and the relative large size of iodide (2.20 Å).[24] Contrasting the Ca1–N1 and Ca2–N2 bonds (2.440(3) Å and 2.385(3) Å), which also reflect the differences, the Ca1–N3 and Ca2–N4 bonds are almost identical with 2.401(3) Å and 2.405(3) Å.

Reactivity

The differences in the reduction behaviour of NDI by alkali and alkaline earth metals raise the question of whether these differences also extend to their reactivity. Generating Na_2NDI *in situ* in toluene affords a dark brownish yellow solution. A subsequent reaction with 2 equivalents of AlI_3 in toluene results in $[\{AlI_2\}_2(NDI)]$ (**6**) as a dark red solid in moderate yield (Scheme 4). Due to the fact, that the reduced naphthyridine-backbone is maintained in this reaction, the ^1H NMR spectrum shows a similar set of highly upfield shifted doublets as before (Fig. S7, 5.94 ppm and 5.10 ppm). This behaviour is also consistent with observations made for other reduced NDI metal complexes.[12,16,18] The molecular structure of compound **6** was determined by XRD (Fig. 7, top). Each moiety in compound **6** contains an aluminium centre which adapts a dis-

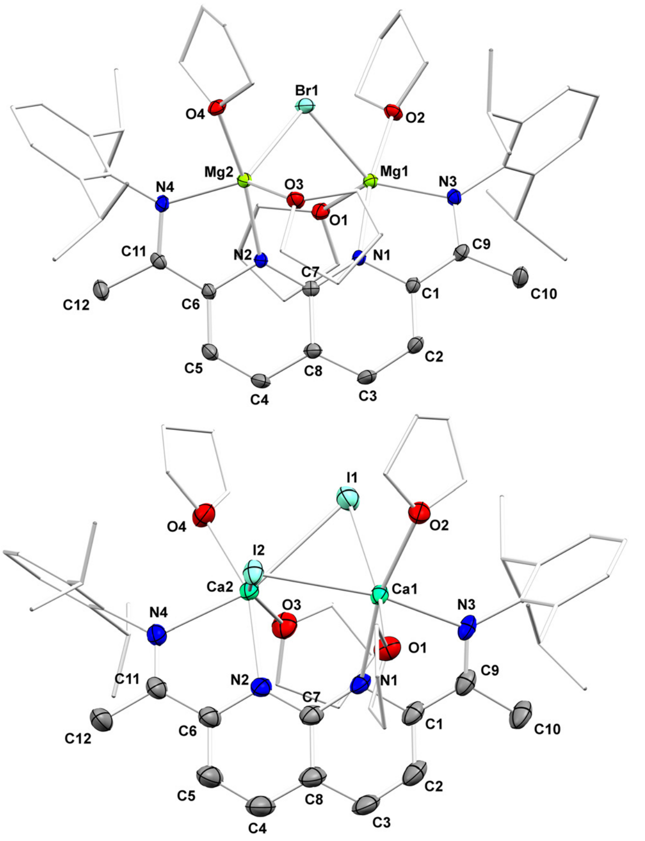

Fig. 6 Molecular structure of complex **4** (top) and **5** (bottom). All atoms are represented by atomic displacement ellipsoids set at 50% probability. Solvent molecules and hydrogen atoms are omitted for clarity. Carbon atoms of the coordinating solvent and substituents are displayed in a capped stick model. Selected interatomic distances (Å): Mg1–N1 2.107(2), Mg1–N3 2.049(2), Mg2–N2 2.107(2), Mg2–N4 2.049(2), Mg1–Br1 2.573, Mg2–Br1 2.573, N1–C1 1.421(3), C1–C9 1.388(4), N3–C9 1.384(4), N2–C6 1.421(3), C6–C11 1.388(4), N4–C11 1.384(4), C2–C3 1.362(4), C4–C5 1.362(4), C7–C8 1.451(5); Ca1–N1 2.440(3), Ca1–N3 2.401(3), Ca2–N2 2.385(3), Ca2–N4 2.405(3), N1–C1 1.422(5), C1–C9 1.420(6), N3–C9 1.327(5), N2–C6 1.400(4), C6–C11 1.431(5), N4–C11 1.318(5), C2–C3 1.361(6), C4–C5 1.372(6), C7–C8 1.450(5) (for further metrics, see SI).

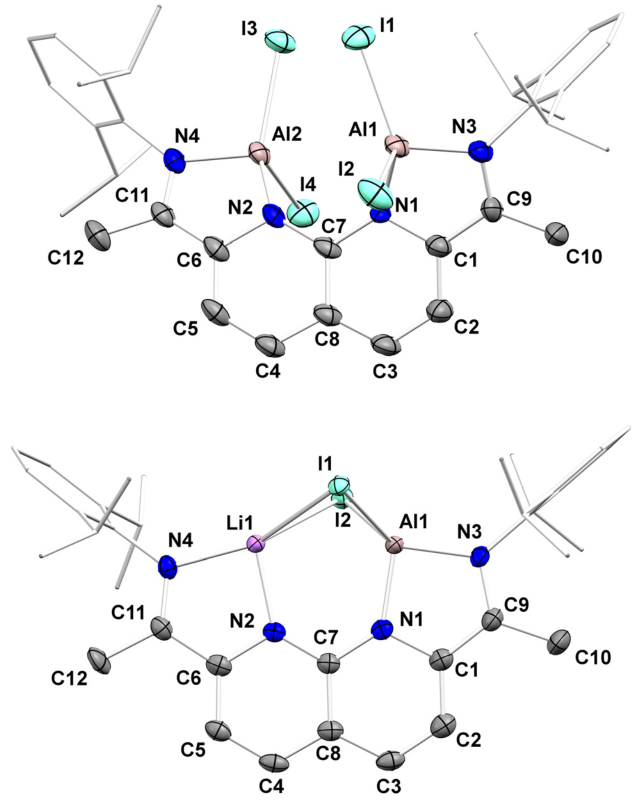

Fig. 7 Molecular structure of complex **6** (top) and **7** (bottom). All atoms are represented by atomic displacement ellipsoids set at 50% probability. Solvent molecules and hydrogen atoms are omitted for clarity. Carbon atoms of the coordinating solvent and substituents are displayed in a capped stick model. Selected interatomic distances (Å): Al1–N1 1.919(5), Al1–N3 1.874(5), Al2–N2 1.925(6), Al2–N4 1.868(5), Al1–I1 2.525(2), Al1–I2 2.464(2), Al2–I3 2.501(2), Al2–I4 2.531(2), N1–C1 1.421(7), C1–C9 1.412(7), N3–C9 1.350(8), N2–C6 1.421(6), C6–C11 1.408(7), N4–C11 1.347(9), C2–C3 1.366(9), C4–C5 1.366(9), C7–C8 1.438(8); Al1–N1 1.827(3), Al1–N3 1.836(3), Li1–N2 2.00(4), Li1–N4 1.95(6), Al1–I1 2.574(2), Al1–I2 2.564(2), Li1–I1 2.85(5), Li1–I2 2.94(6), N1–C1 1.421(4), C1–C9 1.394(5), N3–C9 1.376(4), N2–C6 1.385(4), C6–C11 1.463(4), N4–C11 1.317(4), C2–C3 1.349(5), C4–C5 1.383(5), C7–C8 1.440(4) (for further metrics, see SI).

torted tetrahedral geometry with two iodides. The most significant distortion is the obtuse N1/N2–Al–I angle with a mean of 136.6°, oriented along the Al–Al axis. Nevertheless, the Al–Al distance (4.165(2) Å) is larger than twice the covalent radius of aluminium (1.21 Å), as well as examples found in literature (2.5–2.95 Å), indicating the absence of an Al–Al bond.[32,33] If the reaction is conducted with 2 equivalents of $GaCl_3$, a homobimetallic Ga_2NDI species is formed. But this species seems to react further with the produced metathesis salt to form $[Na_2(GaCl_4)_3][\{(GaCl_2)_2\}(NDI)]$ (see SI for further information). As the subsequent reaction with the metathesis salt could not be suppressed despite numerous attempts under various con-

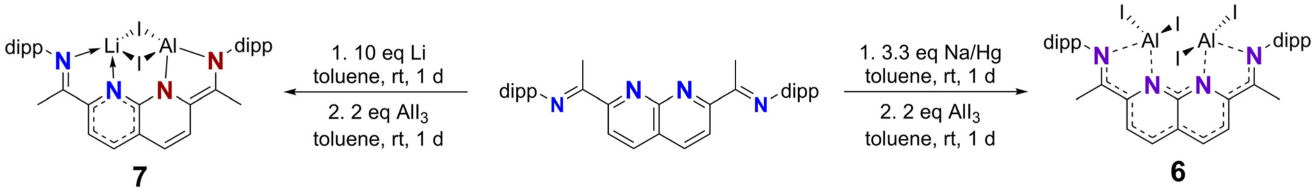

Scheme 4 Reactions of NDI, pre-reduced with granular lithium or sodium amalgam, and AlI_3.

ditions, and the resulting complex does not correspond to the desired product, it is not considered further in this discussion.

The reactivity of NDI reduced by lithium towards AlI_3 reveals a preference for the formation of heterobimetallic complexes, even though 2 equivalents of AlI_3 are being used. Performing the reaction with AlI_3 in toluene (to ensure that **2c** is formed as the main intermediate) selectively yields deep green [{(Al)(Li)}(μ-I)$_2$(NDI)] (**7**) (Scheme 4). In the ^{1}H NMR spectrum of complex **7** (Fig. S10), multiple sets of characteristic upfield shifted doublets (6.14 ppm, 5.87 ppm, and 5.33 ppm) can be observed similarly to complex **6**, which are explained by the asymmetry of the complex. Slow evaporation of a *n*-pentane solution results in dark green crystals of compound **7**, suitable for XRD measurements. The crystal structure (Fig. 7, bottom) reveals that the moiety between of N1 and N3 is occupied by one aluminium atom and the other by one lithium atom, with two bridging iodides. Both metal centres display distorted tetrahedral coordination. The Al–N bonds are with an average of 1.832 Å shorter than the ones found in [AlI_2(^{Ar}DAB)]$^+$ (1.92 Å, dative) and [AlI_2(^{Ar}DAB)] (1.89 Å, partially covalent), where either no or one negative charge is delocalised along the NCCN bonds.[34] In [(AlI)(PDI)], one of the two negative charges predominantly remains at the pyridine nitrogen, resulting in a bond length of 1.82 Å for the Al1–N1 bond.[35] This is more consistent with the bond lengths observed in compound **7**. Moreover, the Li–I bonds are unequal with 2.94(6) Å and 2.85(5) Å, indicating LiI character. Therefore, both additional electrons are located at the aluminium centre. Comparing complex **6** to **7**, the Al–N bonds are elongated, indicating more covalent character towards the imine nitrogen atoms (Al–N1/N2 1.922 Å, Al–N3/N4 1.871 Å). Additionally, in contrast to complex **7**, the metal centres in complex **6** are tilted by about 25.0° on average out of the mean NCCN plane. A break in planarity can be observed for the naphthyridine-backbone with the two mean planes of the individual pyridine rings, spanning an angle of 11.4°. This distorted-backbone is another indication of the previously mentioned de-aromatisation of reduced NDI metal complexes.

Investigating the formation of heterobimetallic complexes further, we utilised lithium reduced NDI and 2 equivalents of $GaCl_3$ in toluene (Scheme 5). Deep green [{(GaCl)(Li(thf)$_2$)}(μ-Cl)(NDI)] (**8**) can be isolated by extraction with *n*-pentane. A ^{1}H NMR spectrum of compound **8** (Fig. S14) reveals a more complex situation in solution. Several signal pairs corresponding to NDI units in different magnetic environments are observable. But the environments must be regular, as only one sharp signal at 1.93 ppm can be seen in the ^{7}Li NMR spectrum (Fig. S15). XRD measurements of compound **8** (Fig. 8, top) reveal a monomeric structure in the solid-state with one lithium and one gallium atom occupying each one of the moieties. The lithium centre is analogous to the magnesium centre in complex **4**, displaying a bipyramidal geometry with the imine nitrogen and the oxygen atom from THF at the apical positions. The gallium centre is bound to two nitrogen atoms and two chlorides (bridging and terminal), resulting in a tetrahedral geometry. The Ga–N bond lengths of comparable gallium halide complexes with redox-active ligands range from around 2.17 Å (mostly dative with neutral ligand) to 1.89 Å (more covalent with anionic ligands).[34–39] In complex **8**, the Ga–N bond lengths are with 1.890 Å on the lower end, indicative of the stronger delocalisation along the NCCN bond like in complex **7**.

Taking the HSAB concept into account, the incomplete exchange in the metathesis reactions with lithium can be partially contributed to a good match of hardness between lithium and nitrogen. The formation of aggregates, like in the complexes **2a**–**2c**, suggests this as well. Additionally, side reactions caused by solvated Li-atoms outside the NDI centre and varying possible charges with different species of lithium further explain the preference for heterometallic binuclear complexes.

Here, it has to be mentioned, that the reaction of NDI reduced by lithium with $GaCl_3$ further proves the complexity of the pre-reduction step with lithium, since we were able to isolate monometallic [($GaCl_2$)(NDI)] (**9**) as NMR-silent minor side product. This formation could be attributed to minor impurities during the *in situ* generation of **2c** or the decomposition of complex **8**. However, up to this point, we were unable to selectively transform complex **8** to **9** *via* thermal decomposition. Nevertheless, [($GaCl_2$)(NDI)] (**9**) can be selectively syn-

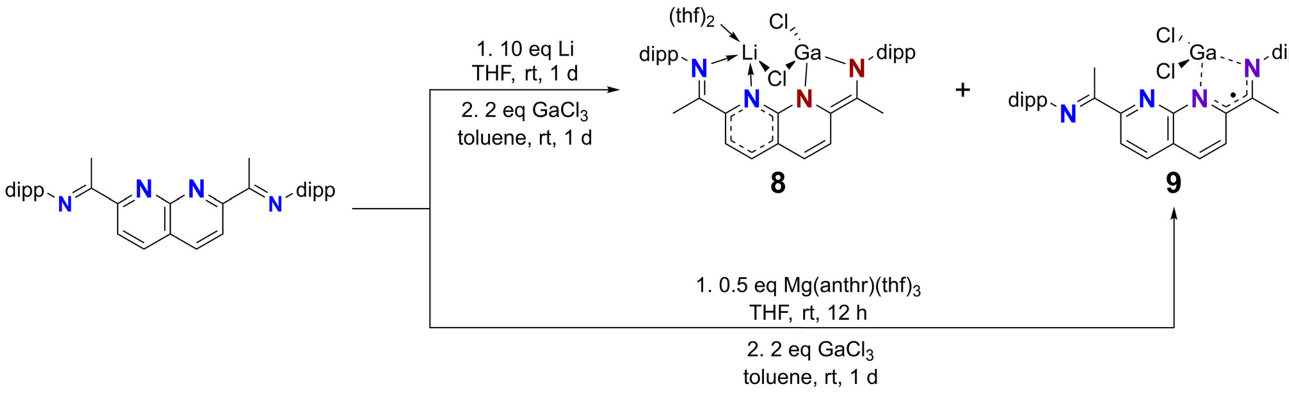

Scheme 5 Reaction of with lithium pre-reduced NDI and $GaCl_3$, and an alternative route *via* pre-reducing with Mg(anthr)(thf)$_3$.

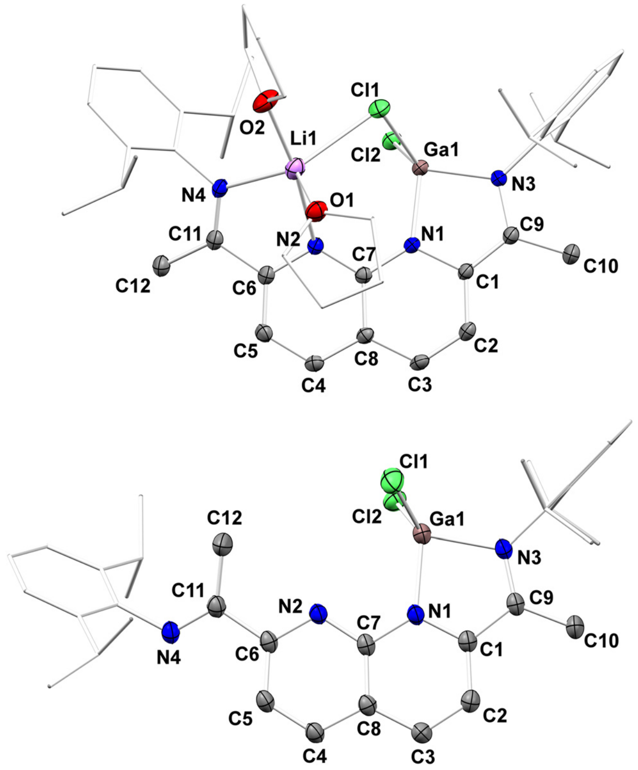

Fig. 8 Molecular structure of complex **8** (top) and **9** (bottom). All atoms are represented by atomic displacement ellipsoids set at 50% probability. Solvent molecules and hydrogen atoms are omitted for clarity. Carbon atoms of the coordinating solvent and substituents are displayed in a capped stick model. Selected interatomic distances (Å): Ga1–N1 1.889(2), Ga1–N3 1.891(2), Li1–N2 2.297(6), Li1–N4 2.111(3), Ga1–Cl1 2.1935(8), Ga1–Cl2 2.1966(5), Li1–Cl1 2.508(3), N1–C1 1.428(3), C1–C9 1.372(2), N3–C9 1.399(3), N2–C6 1.362(2), C6–C11 1.484(3), N4–C11 1.287(3), C2–C3 1.355(2), C4–C5 1.403(4), C7–C8 1.435(3); Ga1–N1 1.915(2), Ga1–N3 1.954(1), Ga1–Cl1 2.1610(6), Ga1–Cl2 2.1448(7), N1–C1 1.373(3), C1–C9 1.433(3), N3–C9 1.328(3), N2–C6 1.340(2), C6–C11 1.489(3), N4–C11 1.282(3), C2–C3 1.367(3), C4–C5 1.377(3), C7–C8 1.417(4) (for further metrics, see SI).

thesised by utilising the magnesium precursor **3** with 2 equivalents of GaCl$_3$ in toluene (Scheme 5). The structure motif (Fig. 8, bottom) is similar to the ones of complexes **1** and **3**. The gallium centre is bonded to two nitrogen and two chlorine atoms, displaying a distorted tetrahedral geometry. The Ga1–N1 and Ga1–N3 bonds are elongated (1.915(2) Å and 1.954(1) Å), compared to complex **8**. In contrast to **8**, where the N1–Ga1–N3 plane is tilted by 7.80° out of the N1–C1–C9–N3 mean plane, it is tilted by 1.28° for complex **9**.

Another example highlighting the difference between the pre-reduction with lithium and that with sodium is the reaction with 2 equivalents of CaI$_2$. While the formation of the homobimetallic complex **5** is observed with sodium, the same reaction conditions using lithium yield a different product. The ^{1}H NMR spectrum of the isolated product (Fig. S16) contains sets of signals corresponding to asymmetric species, as well as unreacted precursor. This is also supported by the ^{7}Li NMR spectrum (Fig. S17), where several signals different from the precursor can be observed. No traces of complex **5** are detected, further indicating that pre-reduction with lithium favors the formation of heterobimetallic complexes. Further indication comes from an analogous reaction with CaCl$_2$, which yielded a few crystals of a dimeric [CaCl(thf)$_2$(NDI)]$_2$ complex (see SI for further information). This outcome could be explained by the decomposition of a heterobimetallic NDI complex into elemental lithium and the isolated product.

Structural categorisation

In the work of the group of Uyeda,[16] bond lengths were also investigated within the NDI framework. They were able to reveal a trend between the bond lengths of the framework and the formal number of electrons at the metal centre. Additionally, regarding the bond lengths, the group of de Bruin analysed those in diazabutadiene (DAD) complexes from the Cambridge Crystallographic Data Center (CCDC) database.[40] According to a metrical oxidation state (MOS) model, they found a correlation between the bond lengths and the oxidation state of the redox-active ligand, independent from the complexed metal. Intrigued by the similarity of NDI to DAD, the metrics of the available crystallographic data of monomeric NDI complexes were analysed with the intent to reveal an analogous trend. This trend in turn could give a data-based indication of the formal oxidation state of NDI, and consequently the metal centres in both hetero- and homo-bimetallic complexes.

The bond lengths were sorted, with the C1–C9 bond being shorter than the C6–C11 bond. Structural considerations, based on comparing crystallographic data and possible resonance structures (Scheme 6) made clear that the bonds of C1–C9 and C6–C11 are sufficient for a qualitative statement of the formal oxidation state for NDI^n (0 ≥ n > 3−). This is rooted in the delocalisation along the NCCN bonds, analogous to DAD complexes. The two bonds in question are sp^2–sp^2 hybridised C–C bonds with a typical bond length of 1.47 Å for a single

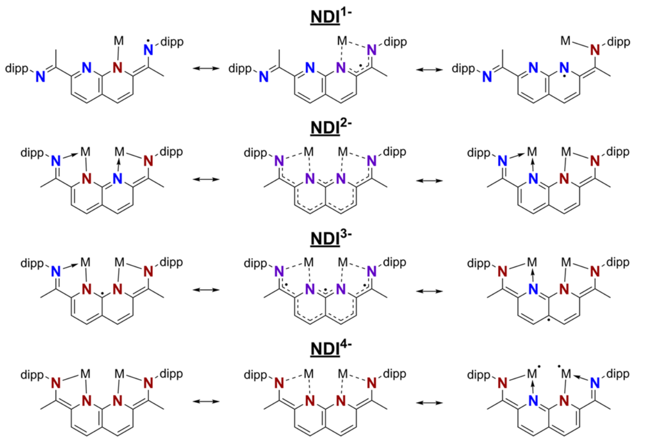

Scheme 6 Structural considerations for the reduction of NDI^n (1− ≥ n ≥ 4−).

bond, 1.40 Å for a delocalised bond and 1.32 Å for a double bond.[41] Focussing only on the metrics, a charge of 0 or larger per DAD subunit is assigned for a C1–C9/C6–C11 bond length greater than 1.47 Å. If the bond length is between 1.47 Å and 1.40 Å, each bond is counted towards the NDI framework being reduced once. The resulting plot can be found in Fig. 9.

Bonds longer than 1.47 Å can be found in the free NDI (1.494(2) Å, 1.500(2) Å, $n = 0$), as well as for the oxidised cases ($n = +1$).[12] In the asymmetric monometallic case of complex **1**, the C1–C9 bond with 1.456(2) Å indicates a charge of 1− for the respective unit and the C6–C11 bond with 1.486(3) Å a charge of 0. The resulting formal oxidation state of NDI^{1-} agrees with the countering Na^+ centre. The same applies to complex **3**, where bond lengths of 1.440(2) Å and 1.490(2) Å can be found. Furthermore, the literature known binuclear homometallic [{(CoCl)(CoCl(thf))}(μ-Cl)(NDI)] falls into the same category (1.435(6) Å and 1.471(7) Å), where the charge analysis indicates a NDI^{1-} fragment as well.[16]

One seemingly unfitting complex is $[\{Ni_2(C_6H_6)\}\{K(thf)_3\}(NDI)]$ (**A3** in Fig. 9), the product of $[\{Ni_2(C_6H_6)\}(NDI)]$ being reduced with 1 equivalent of KC_8.[12] At first glance, a reduction from NDI^{2-} to NDI^{3-} would be expected. But DFT calculations revealed that the additional electron is mostly located in metal-centred orbitals, thus formally maintaining NDI^{2-}.[12] The trend therefore still applies. Complexes [{(CoCl)(CoCl(thf))}(μ-Cl)(NDI)] and [{(FeCl)(FeCl(thf))}(μ-Cl)(NDI)] (**B1** and **B2** in Fig. 9) are extreme cases, falling into either the NDI^{1-} or NDI^{2-} case, based on their uncertainties. Turning towards complex **7**, it is the first binuclear heterometallic complex with this specific NDI framework. Assuming each subunit carries a charge of −2 for bonds shorter than 1.40 Å, this would incorrectly imply a total NDI charge of −3 (1.394(5) Å and 1.463(4) Å). But due to the symmetric nature of complex **7**, the crystallographic data may exhibit partial disorder between aluminium and lithium sites. To minimise influences on the NDI framework, compound **7-thf** (Fig. S42) was crystallised out of a *n*-pentane solution of compound **7** with a few drops of THF (see SI). The differences in complex **7-thf** are more pronounced with 1.365(8) Å for the C1–C9 bond at the aluminium and 1.488(6) Å for the C6–C11 bond at the lithium centre. Corresponding to a total NDI charge of −2, 0 for the lithium site and −2 for the aluminium site. The larger charge at the imine nitrogen N4 results in a greater contribution of a N–C single and C–C double bond. This is also indicated by the elongated N4–C11 bond length, from 1.286(7) Å for the free NDI to 1.399(6) Å.[12]

Describing a subunit with a charge of 2− for bonds shorter than 1.40 Å is on one hand in accordance with the description of NDI^{4-} for the binuclear homometallic $[Ge_2NDI]$ complex of Braunschweig with 1.384(3) Å for both bonds.[18] On the other hand, the same description results for complex **4** in NDI^{4-}, whereas only a total charge of −3 is the most reasonable description. A possible approach to differentiate between NDI^{3-} and NDI^{4-} in a binuclear case resulted from the comparison of the C7–C8 bond length (Fig. 10). They range from around 1.40 to 1.45 Å. Neutral or positively charged NDI frameworks are located at the lower end, reduced species without further distinction at the higher end. Interestingly, the longest bond is found in complex **4** with 1.451(5) Å, but the $[Ge_2NDI]$ complex with NDI^{4-} demonstrates the shortest one with 1.397(3) Å.[18] This can be explained by looking at the resonance structures of the NDI framework (Scheme 6), depending on the

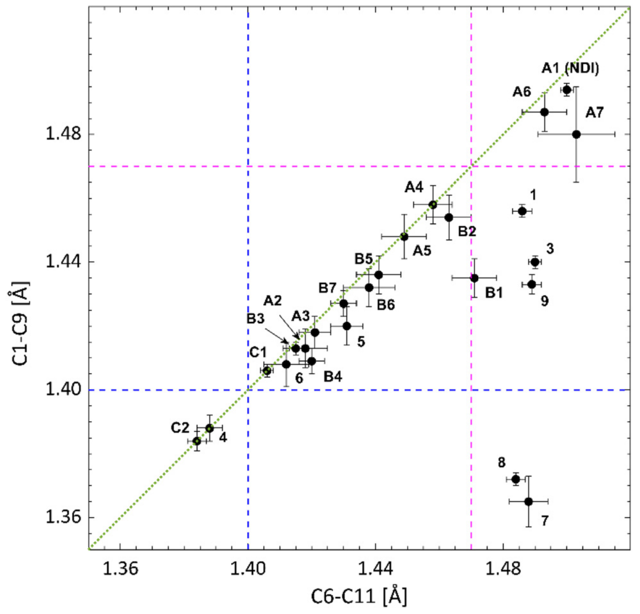

Fig. 9 Bond length of the C1–C9 bond against the C6–C11 bond. Trend for being reduced once for values lower than 1.47 Å (magenta dashed line), and for being reduced twice for lower than 1.40 Å (blue dashed line). Along the first angle bisector (green dotted line) indicates higher symmetry. See SI (Table S7) for the full set of data points.

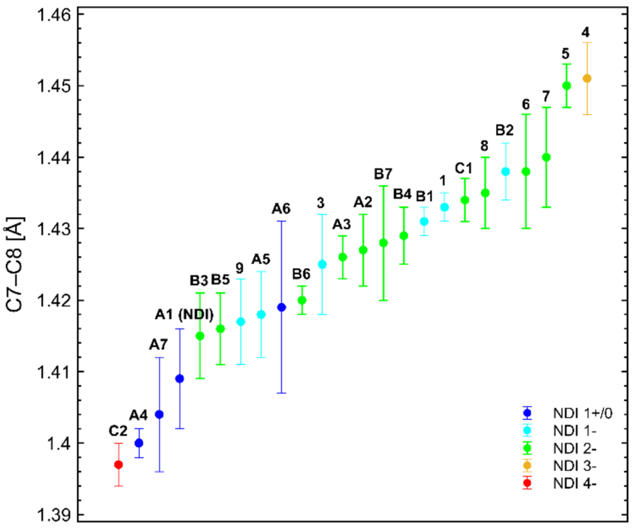

Fig. 10 Bond length of the C7–C8 bond in NDI complexes in varying formal oxidation states. Trend to differentiate between three-time (>1.45 Å) and four-time reduction (<1.40 Å) of NDI. See SI (Table S7) for the full set of data points.

degree of reduction. They reveal that the largest contributions of a C7–C8 double bond are present in the cases of NDI^n with $n \geq 0$ or $n = 4-$. In the cases of $0 > n > 4-$, most resonance structures contain more contributions towards a C7–C8 single bond, resulting in the elongated bonds observed.

Conclusions

Our investigations reveal that ligand pre-reduction is not merely a preparative step but a decisive factor in dictating the structure and electronic properties of NDI-based complexes. By systematically exploring different reductants and conditions, we uncovered a spectrum of reactivity patterns, highlighting how subtle changes guide the formation of monometallic or homo- and heterobimetallic species. The contrasting behaviours observed between alkali and alkaline earth metals emphasise the nuanced interplay between different factors like ligand charge, coordination environment, and metal identity. Moreover, a model, inspired by the chemistry of diazabutadiene ligands, for assessing NDI oxidation states provides a valuable tool for interpreting redox behaviour across a growing library of related systems. This work not only expands the synthetic utility of NDI ligands but also provides a conceptual basis for future design of multimetallic complexes with tuneable electronic structures. Building on these insights, our ongoing efforts focus on extending this approach to early transition and rare earth metals.

Author contributions

A. J., synthesis and characterisation of compounds, writing original draft; L. N., synthesis of compounds; H. S. and C. M.-M., crystallography; M. M. conceptualisation, supervision, writing and project administration. All authors contributed to the finalisation of the manuscript and agreed to the submitted content.

Conflicts of interest

There are no conflicts to declare.

Data availability

The data that support the findings of this study are available in the SI of this manuscript. Included are synthetic and characterizing data, representative spectra, details of the X-ray crystal structures and quantum chemical calculations. The authors have cited additional references within the SI. See DOI: https://doi.org/10.1039/d5qi01216c.

CCDC 2453329–2453340, 2453364 and 2472914 contain the supplementary crystallographic data for this paper.[42a–n]

Acknowledgements

Financial support (VCI Liebig fellowship for A. J. and M. M.) is gratefully acknowledged. M. M. further wishes to acknowledge the Vector Stiftung for financial support and Prof. Reiner Anwander for his continuous support and guidance.

References

1 M. H. Pérez-Temprano, J. A. Casares, A. R. de Lera, R. Álvarez and P. Espinet, Strong Metallophilic Interactions in the Palladium Arylation by Gold Aryls, *Angew. Chem., Int. Ed.*, 2012, **51**, 4917–4920.

2 C. Chen, C. Hou, W. Yuguang, T. S. A. Hor and Z. Weng, Copper-Catalyzed Trifluoromethylselenolation of Aryl and Alkyl Halides: The Silver Effect in Transmetalation, *Org. Lett.*, 2014, **16**, 524–527.

3 R. J. Oeschger and P. Chen, Structure and Gas-Phase Thermochemistry of a Pd/Cu Complex: Studies on a Model for Transmetalation Transition States, *J. Am. Chem. Soc.*, 2017, **139**, 1069–1072.

4 J. Fritsch, P. Scheerer, S. Frielingsdorf, S. Kroschinsky, B. Friedrich, O. Lenz and C. M. T. Spahn, The crystal structure of an oxygen-tolerant hydrogenase uncovers a novel iron-sulphur centre, *Nature*, 2011, **479**, 249–252.

5 S.-J. Xie, R.-K. Wu, Y.-F. Huang, H.-L. Chen, S.-Q. Zhang, F. Liu, D.-D. Zhai, X. Hong and Z.-J. Shi, Direct Incorporation of Dinitrogen into an Aliphatic C–H Bond, *J. Am. Chem. Soc.*, 2023, **145**, 6773–6780.

6 J. P. Stambuli, R. Kuwano and J. F. Hartwig, Unparalleled Rates for the Activation of Aryl Chlorides and Bromides: Coupling with Amines and Boronic Acids in Minutes at Room Temperature, *Angew. Chem., Int. Ed.*, 2002, **41**, 4746–4748.

7 T. Ooi, M. Takahashi, M. Yamada, E. Tayama, K. Omoto and K. Maruoka, (2,7-Disubstituted-1,8-biphenylenedioxy) bis(dimethylaluminum) as Bidentate Organoaluminum Lewis Acids: Elucidation and Synthetic Utility of the Double Electrophilic Activation Phenomenon, *J. Am. Chem. Soc.*, 2004, **126**, 1150–1160.

8 D. C. Powers, D. Benitez, E. Tkatchouk, W. A. Goddard III and T. Ritter, Bimetallic Reductive Elimination from Dinuclear Pd(III) Complexes, *J. Am. Chem. Soc.*, 2010, **132**, 14092–14103.

9 J. Campos, Bimetallic cooperation across the periodic table, *Nat. Rev. Chem.*, 2020, **4**, 696–702.

10 Q. Wang, S. H. Brooks, T. Liu and N. C. Tomson, Tuning metal–metal interactions for cooperative small molecule activation, *Chem. Commun.*, 2021, **57**, 2839–2853.

11 E. Braconi and N. Cramer, A Chiral Naphthyridine Diimine Ligand Enables Nickel-Catalyzed Asymmetric Alkylidenecyclopropanations, *Angew. Chem., Int. Ed.*, 2020, **59**, 16425–16429.

12 Y.-Y. Zhou, D. R. Hartline, T. J. Steiman, P. E. Fanwick and C. Uyeda, Dinuclear Nickel Complexes in Five States of

Oxidation Using a Redox-Active Ligand, *Inorg. Chem.*, 2014, **53**, 11770–11777.

13 T. J. Steiman and C. Uyeda, Reversible Substrate Activation and Catalysis at an Intact Metal–Metal Bond Using a Redox-Active Supporting Ligand, *J. Am. Chem. Soc.*, 2015, **137**, 6104–6110.

14 I. G. Powers, J. M. Andjaba, X. Luo, J. Mei and C. Uyeda, Catalytic Azoarene Synthesis from Aryl Azides Enabled by a Dinuclear Ni Complex, *J. Am. Chem. Soc.*, 2018, **140**, 4110–4118.

15 A. K. Maity, A. E. Kalb, M. Zeller and C. Uyeda, A Dinickel Catalyzed Cyclopropanation without the Formation of a Metal Carbene Intermediate, *Angew. Chem., Int. Ed.*, 2021, **60**, 1897–1902.

16 M. J. Behlen, Y.-Y. Zhou, T. J. Steiman, S. Pal, D. R. Hartline, M. Zeller and C. Uyeda, Dinuclear oxidative addition reactions using an isostructural series of Ni_2, Co_2, and Fe_2 complexes, *Dalton Trans.*, 2017, **46**, 5493–5497.

17 K. B. Brook, S. R. Sahoo and C. Uyeda, Dicobalt-catalyzed N=N coupling reactions of tertiary alkyl azides to form azoalkanes, *Chem*, 2025, **11**, 102437.

18 J. Cui, J. Weiser, F. Fantuzzi, M. Dietz, Y. Yatsenko, A. Häfner, S. Nees, I. Krummenacher, M. Zhang, K. Hammond, P. Roth, W. Lu, R. D. Dewhurst, B. Engels and H. Braunschweig, A rigid redox-active-ligand-supported bis(germylene) as a two-centre six-electron donor, *Chem. Commun.*, 2022, **58**, 13357–13360.

19 E. Kounalis, R. Sieben, L. Witteman, M. Lutz, M.-E. Moret and D. L. J. Broere, An N-Heterocyclic germylene with a versatile metal-binding pocket: insights into hetero-dinuclear bonding and reactivity, *Chem. Sci.*, 2025, **16**, 12613–12622.

20 N. L. Bazyakina, M. V. Moskalev, A. V. Cherkasov, V. M. Makarov and I. L. Fedushkin, Coordination polymers derived from alkali metal complexes of redox-active ligands, *CrystEngComm*, 2022, **24**, 2297–2304.

21 J. Scott, I. Vidyaratne, I. Korobkov, S. Gambarotta and P. H. M. Budzelaar, Multiple Pathways for Dinitrogen Activation during the Reduction of an Fe Bis(iminepyridine) Complex, *Inorg. Chem.*, 2008, **47**, 896–911.

22 R. E. Mulvey, MELDOLA MEDAL LECTURE: Ring-Stacking and Ring-Laddering in Organonitrogenlithium Compounds: The Development of Concepts with Wide Applicability throughout Lithium Structural Chemistry, *Chem. Soc. Rev.*, 1991, **20**, 167–209.

23 R. E. Mulvey, Synthetic and structural developments in hetero-s-block-metal chemistry: new ring-laddering, ring-stacking and other architectures, *Chem. Soc. Rev.*, 1998, **27**, 339–346.

24 R. D. Shannon, Revised Effective Ionic Radii and Systematic Studies of Interatomic Distances in Halides and Chalcogenides, *Acta Crystallogr., Sect. A*, 1976, **32**, 751–767.

25 J. Gao, Y. Liu, Y. Zhao and Y. Sui, Syntheses and Structures of Magnesium Complexes with Reduced α-Diimine Ligands, *Organometallics*, 2011, **30**, 6071–6077.

26 C. Weetman, M. S. Hill and M. F. Mahon, Magnesium-catalysed hydroboration of pyridines: Kinetic analysis and poly-pyridine dearomatisation, *Polyhedron*, 2016, **103**, 115–120.

27 I. L. Fedushkin, V. A. Chudakova, A. A. Skatova and G. K. Fukin, Solvent-free alkali and alkaline earth metal complexes of di-imine ligands, *Heteroat. Chem.*, 2005, **16**, 663–670.

28 B. Bogdanović, S.-T. Liao, R. Mynott, K. Schlichte and U. Westeppe, Rate of Formation and Characterization of Magnesium Anthracene, *Chem. Ber.*, 1984, **117**, 1378–1392.

29 T. Alonso, S. Harvey, P. C. Junk, C. L. Raston, B. W. Skelton and A. H. White, Main Group-Conjugated Organic Anion Chemistry. 1. Synthesis of Magnesium Anthracene, Silylated Anthracenes, or Fluoranthene Tetrahydrofuran and Tertiary Amine Complexes and of Magnesium Cyclooctatetraene: X-ray Structure of [MgL(TMEDA)]·[MgL(THF)$_2$] (L = 9,10-Bis(trimethylsilyl)anthracene), *Organometallics*, 1987, **6**, 2110–2116.

30 S. P. Green, C. Jones and A. Stasch, Stable Magnesium(I) Compounds with Mg-Mg Bonds, *Science*, 2007, **318**, 1754–1757.

31 S. P. Green, C. Jones and A. Stasch, Stable Adducts of a Dimeric Magnesium(I) Compound, *Angew. Chem., Int. Ed.*, 2008, **47**, 9079–9083.

32 B. Cordero, V. Gómez, A. E. Platero-Prats, M. Revés, J. Echeverría, E. Cremades, F. Barragán and S. Alvarez, Covalent radii revisited, *Dalton Trans.*, 2008, 2832–2838.

33 P. Bag, C. Weetman and S. Inoue, Experimental Realisation of Elusive Multiple-Bonded Aluminium Compounds: A New Horizon in Aluminium Chemistry, *Angew. Chem., Int. Ed.*, 2018, **57**, 14394–14413.

34 R. J. Baker, R. D. Farley, C. Jones, M. Kloth and D. M. Murphy, The reactivity of diazabutadienes toward low oxidation state Group 13 iodides and the synthesis of a new gallium(I) carbene analogue, *J. Chem. Soc., Dalton Trans.*, 2002, 3844–3850.

35 T. M. Bass, C. R. Carr, T. J. Sherbow, J. C. Fettinger and L. A. Berben, Syntheses of Square Planar Gallium Complexes and a Proton NMR Correlation Probing Metalloaromaticity, *Inorg. Chem.*, 2020, **59**, 13517–13523.

36 Y. Liu, S. Li, X.-J. Yang, Q.-S. Li, Y. Xie, H. F. Schaefer and B. Wu, Alkali metal compounds of a gallium(I) carbene analogue {:Ga[N(Ar)C(Me)]$_2$} (Ar = 2,6-^{i}Pr$_2$C$_6$H$_3$), *J. Organomet. Chem.*, 2011, **696**, 1450–1455.

37 Y. Zhao, Y. Liu, Q.-S. Li and J.-H. Su, Synthesis and structures of mononuclear and dinuclear gallium complexes with α-diimine ligands: reduction of the metal or ligand?, *Dalton Trans.*, 2016, **45**, 246–252.

38 I. L. Fedushkin, V. A. Dodonov, A. A. Skatova, V. G. Sokolov, A. V. Piskunov and G. K. Fukin, Redox-Active Ligand-Assisted Two-Electron Oxidative Addition to Gallium(II), *Chem. – Eur. J.*, 2018, **24**, 1877–1889.

39 M. Schorpp, R. Tamim and I. Krossing, Oxidative addition, reduction and reductive coupling: the versatile reactivity of subvalent gallium cations, *Dalton Trans.*, 2021, **50**, 15103–15110.

40 F. J. de Zwart, B. Reus, A. A. H. Laporte, V. Sinha and B. de Bruin, Metrical Oxidation States of 1,4-Diazadiene-Derived Ligands, *Inorg. Chem.*, 2021, **60**, 3274–3281.

41 M. A. Fox and J. K. Whitesell, *Organische Chemie*, Spektrum Akademischer Verlag, Heidelberg, Berlin, 1995.

42 (*a*) C. Maichle-Mössmer, CCDC 2453329: Experimental Crystal Structure Determination, 2025, DOI: **10.5517/ccdc.csd.cc2nbwnk**; (*b*) C. Maichle-Mössmer, CCDC 2453330: Experimental Crystal Structure Determination, 2025, DOI: **10.5517/ccdc.csd.cc2nbwpl**; (*c*) C. Maichle-Mössmer, CCDC 2453331: Experimental Crystal Structure Determination, 2025, DOI: **10.5517/ccdc.csd.cc2nbwqm**; (*d*) C. Maichle-Mössmer, CCDC 2453332: Experimental Crystal Structure Determination, 2025, DOI: **10.5517/ccdc.csd.cc2nbwrn**; (*e*) C. Maichle-Mössmer, CCDC 2453333: Experimental Crystal Structure Determination, 2025, DOI: **10.5517/ccdc.csd.cc2nbwsp**; (*f*) C. Maichle-Mössmer, CCDC 2453334: Experimental Crystal Structure Determination, 2025, DOI: **10.5517/ccdc.csd.cc2nbwtq**; (*g*) C. Maichle-Mössmer, CCDC 2453335: Experimental Crystal Structure Determination, 2025, DOI: **10.5517/ccdc.csd.cc2nbwvr**; (*h*) C. Maichle-Mössmer, CCDC 2453336: Experimental Crystal Structure Determination, 2025, DOI: **10.5517/ccdc.csd.cc2nbwws**; (*i*) C. Maichle-Mössmer, CCDC 2453337: Experimental Crystal Structure Determination, 2025, DOI: **10.5517/ccdc.csd.cc2nbwxt**; (*j*) C. Maichle-Mössmer, CCDC 2453338: Experimental Crystal Structure Determination, 2025, DOI: **10.5517/ccdc.csd.cc2nbwyv**; (*k*) C. Maichle-Mössmer, CCDC 2453339: Experimental Crystal Structure Determination, 2025, DOI: **10.5517/ccdc.csd.cc2nbwzw**; (*l*) C. Maichle-Mössmer, CCDC 2453340: Experimental Crystal Structure Determination, 2025, DOI: **10.5517/ccdc.csd.cc2nbx0y**; (*m*) C. Maichle-Mössmer, CCDC 2453364: Experimental Crystal Structure Determination, 2025, DOI: **10.5517/ccdc.csd.cc2nbxsq**; (*n*) M. Manßen, CCDC 2472914: Experimental Crystal Structure Determination, 2025, DOI: **10.5517/ccdc.csd.cc2p08ff**.